Multiscale light-sheet organoid imaging framework

Gustavo de Medeiros[1,2], Raphael Ortiz[1,2], Petr Strnad[1,3], Andrea Boni[1,3], Francisca Maurer[1] and Prisca Liberali[1,4,*]

[1] Friedrich Miescher Institute for Biomedical Research (FMI) Maulbeerstrasse 66, 4058 Basel.
[2]These authors contributed equally.
[3]Current address: Viventis Microscopy Sàrl, EPFL Innovation Park, Building C, 1015 Lausanne.
[4]University of Basel, Basel, Switzerland
*Correspondence should be addressed to P.L. (prisca.liberali@fmi.ch)

Abstract

We present an imaging framework capable of turning long term light-sheet imaging of organoids into digital organoids. The framework takes advantage of deep learning techniques to faithfully segment single organoids, their lumen, cells and nuclei in 3D and over long periods of time. In parallel, large lineage trees for each organoid are predicted and corrected to iteratively improve the tracking and segmentation performances over time. To visualize the extracted information, we developed a web-based "Digital Organoid Viewer" that allows a unique understanding of the multivariate and multiscale data by linking 2D lineage trees with the corresponding 3D segmentation meshes.

We also backtracked single cells of interest after fixation obtaining detailed information about their history within the entire organoid context. Furthermore, we show nuclei merging events that arise from cytokinesis failure and that these polyploid never reside in the intestinal crypt, hinting at a tissue scale control and feedback on cellular fidelity. Molecularly, these cytokinesis failures depend on a regenerative state of the organoids and are regulated by Lats1 and RXR and we propose a model of tissue integrity by multi-scale check points. This discovery sheds light on the robustness of a regenerative YAP cellular state, questioning the role of polyploidy in intestinal regeneration.

Main

During adult life, organs such as the intestine are challenged to diverse environmental conditions, requiring the tissue to be robust and yet plastic. For instance, during regeneration after damage, surviving cells need to carefully orchestrate a fast and robust regrowth process in coordination with proper shape recovery as well as functional and morphological remodeling. To best overcome the difficulties surrounding the study of these tissue dynamics in inner organs *in vivo*, organoids have become a powerful experimental method owing to their exceptional accessibility and manipulability[1-3]. For the case of the intestinal tract, intestinal organoids grown from single cells functionally recapitulate both the regenerative response of the intestinal epithelium as well as the homeostasis of the *in vivo* intestine[4].

Morphologically, they also recapitulate the main dynamics of crypt formation, making them a unique *in vitro* system[5,6,7,8].

Although with high degree of accessibility, performing live imaging of organoid growth remains a challenge, as it typically requires not only microscopy techniques capable of stable long-term imaging of several samples simultaneously, but also dedicated analysis and processing pipelines that can cope with complex imaging data. Nonetheless, previous work on the live recording of organoid dynamics has focused either on specific biological questions[6,8,9] or on specific isolated tools[10] without a more generalised yet in-depth approach on light-sheet imaging and data analysis. The only current work which aimed at creating a light-sheet organoid imaging platform[11] focused mainly on the determination of culture-wide heterogeneities through a combination of both light-sheet and wide-field techniques. Although showing organoid diversity within the same culture, in-depth cellular multi-scale analysis for each organoid remained lacking.

To fully bridge the gap and provide quantitative information on organoid growth dynamics with in-depth cellular analysis, we here provide a unified multiscale light-sheet imaging framework tailored to live organoid imaging called LSTree. Our framework encompasses pre-processing, automated lineage tracking, segmentation and multivariate feature extraction pipelines which provide multiscale measurements from organoid to single cell levels. By focusing on the development of intestinal organoids, we show that this holistic set of tools allows the combination of whole organoid and single cell features to be analysed simultaneously, having both lineage tree as well as spatial segmentation information presented in a clear and unified way. We demonstrate that our pipeline is compatible with fixation and immunolabeling after live imaging by tracking back cells positive for specific markers and compare the history of these cells with all other cells in the organoid. Further, we use our framework to dissect new biological insights on the role of polyploidy during intestinal organoid growth, and we propose a tissue level check point for tissue integrity that could start explaining the interplay between regeneration and cancer.

Results

Imaging framework for light-sheet microscopy of organoid growth

We developed a multiscale imaging framework that comprehends acquisition, pre-processing, automated tracking, segmentation with further feature extraction as well as visualization dedicated for 3D live imaging. In this work, we applied our framework to live intestinal organoid light-sheet recordings performed with a dual-illumination inverted light-sheet[6] microscope, which utilizes a multi-positioning sample holder system (**Fig. 1a**). In order to image organoid development, we followed previously published protocols[6], FACS sorting single cells from mature organoids and mounting them as 5 uL mix drops with Matrigel on top of a ca. 50 um thick fluorinated ethylene propylene (FEP) foil, which are then covered in medium (**Fig 1b** left and **Methods Section**). We patterned the FEP foil used for mounting in order to create small wells (**Supplementary Figure 1**), allowing better control of the sample position within the holder, while improving reproducibility of experiments by preventing drops from being washed away during medium change of fixation procedures. As previously demonstrated, the microscope we utilized in all demonstrations is capable of imaging live

intestinal organoids for long periods of time[6,8] , as well as acquiring time-lapses of mouse embryonic and gastruloid development[12,13]. However, one important drawback of the system was that the alignment of the illumination beams is done only once, prior to the experiment and irrespective of the position of the sample in the dish or holder. Although sufficient in certain situations (e.g. mouse embryo imaging), imaging of samples embedded and distributed inside a gel suffer from refractive index mismatch between water and Matrigel, as well as from the presence of other obstacles in the light-path (other organoids or debris) and from the curved shape of the sample holder itself. Therefore, to improve recording conditions in every individual sample, we developed a position dependent illumination alignment step. This allows to fine tune the alignment of each of the illumination sheets in respect to the detection plane for every sample position so that best image quality possible can be achieved throughout (**Fig 1b** right). Moreover, to minimize storage needs, acquired images were compressed on the fly (using standard LZW library), and the saved data were then further cropped (**Fig 1c** upper row). To better address low signal-to-noise (SNR) recordings we also added denoising and deconvolution steps. Denoising is done using the Noise2Void scheme[14], with its output sent to a tensor-flow based image deconvolution[15] (https://github.com/hammerlab/flowdec) (**Fig 1c** lower row) using measured PSFs from beads (**Supplementary Note 1** and **Methods Section**).

With these first modules at hand, we imaged organoids expressing Histone 2B and mem9 membrane peptide tagged with mCherry and GFP respectively, recording the growth and development of several organoids for around 4 days starting from single cells up to 4-cell clusters (**Fig 1d** and **Supplementary Movie 1**) every 10 minutes. The collected data comprised of organoids that form both budding and enterocyst phenotypes: whereas budding organoids grow from single cells into mature organoids with both crypt and villus structures, enterocysts, comprised of terminally differentiated enterocytes, do not have crypts as they do not develop Paneth cells required for the establishment of the stem cell niche, a necessary step for crypt formation[6,8].

To extract 3D information of the organoid dynamics throughout growth, we performed partial semi-automatic tracking using the Fiji plugin Mastodon (https://github.com/mastodon-sc/mastodon) on 7 datasets. After that, we extracted initial features based on organoid and single cell segmentation and plotted this data over time, to get a first overview on how these parameters evolved (**Fig 1e**). For example, we noticed large variability in cell division synchronicity, as in some datasets the nuclei number growth over time loses the typical staircase-like behavior already early on. Although epithelium volume growth curves follow that of nuclei number, with the characteristic exponential behavior, nuclei density slightly increases over time. Mean cell volume showed characteristic mitotic peaks, with overall cell volume decrease over time, matching the increase in nuclei density. Interestingly, although initially cell to nuclei volume ratio vary, all datasets converge to common steady state values where the cell volume is ca. 3 to 4 times larger than the nuclear volume. We also observed a consistent change in organoid volume due to medium change during the live recordings (**Supplementary Figure 2** and **Supplementary Note 3**). As this initial assessment of our imaging data showed consistent and reproducible results, and to be able to handle larger dataset more rapidly, we developed a more integrated and automated approach.

Dedicated processing workflow

To make the tools directly accessible, we decided to incorporate all image processing and data analysis modules into a unified framework, named LSTree (https://github.com/fmi-basel/LSTree) and is implemented as a Luigi (https://github.com/spotify/luigi) workflow. As pre-processing first step, the user selects which organoid needs to be cropped on the last frame of a movie and minimal bounding boxes per time-point as well as global bounding boxes are automatically generated for all time-points (**Fig 2a**). We also implemented an interactive tool to review the crops and perform few manual corrections, e.g. to account for large displacement between consecutive frames due to a medium change (**Supplementary Figure 3**). Next, denoising and deconvolution of cropped and registered movies is performed as one combined step.

For the segmentation of organoids, as well as their cells and nuclei, we adopted different segmentation strategies all relying on convolutional neural networks (**Fig 2b**) and utilizing the RDCNet instance segmentation network as a base[16]. Nuclei are segmented in 3D following a deep learning model trained with a mix of complete and partial annotations. A small subset of the frames is fully annotated by manually expanding the labels to the full nuclei, whereas partial annotations rely on the initial tracking performed with Mastodon by drawing spheres at the position of tracked nuclei. (**Fig 2b** upper row). Jupyter notebooks for interactive visualization and correction of the predicted segmentation are also provided, which allows improving the model accuracy with minimal annotating time.

Organoid and cell segmentation also use RDCNet and leverages the pre-computed nuclei segmentation to avoid manual annotations of individual cells. The semantic branch predicts 3 classes (background, lumen and epithelium) and is supervised by manual annotations of a few frames per datasets. To subdivide the epithelium mask into cells, the previously segmented nuclei are used as partial cell annotations under the assumption that they are randomly distributed within the cell compartment (**Fig 2b** lower row, **Supplementary Note 2**). Finally, in addition to the segmentation volumes and nuclei number (**Fig. 1e**), several different features is also extracted such as nuclear distance to apical/basal membranes, fluorescence intensity, distance to parent node, number of neighbors per cell and more (For a complete list of features with short explanations see **Supplementary Table 1**).

Deep learning model for automated lineage tracing

Although suitable for estimating lineage trees for a few datasets, semi-automated tracking of many large datasets with the Mastodon Fiji plugin can be extremely time consuming. To significantly improve this process, we trained and refined a deep learning model on the available tracked datasets to automatically generate candidate trees that only require minimal corrections (**Fig 2c,d, Supplementary Note 2**). The most effective lineage tracing algorithms to date attempt to first detect nuclei and subsequently link them across time while enforcing a complex set of rules[17-19]. We however found that this approach performed poorly on later time-points where the detection accuracy dropped due to the high cell density. We realized that on these challenging cases, even manual nuclei detection requires to take in account the temporal information from neighboring frames. Therefore, we developed a joint segmentation-tracking approach that simultaneously predicts matching nuclei labels on 2 consecutive frames. To this end, we extended the RDCNet instance segmentation model to predict pseudo 4D labels (3D convolutional network with time axis as an additional image

channels) mapping correspondences between nuclei in 2 consecutive frames (**Fig 2c**). Predicting linked nuclei segmentations has the advantage to enforce constancy over the entire nuclear volume rather than relying on an ambiguous center, as well as implicitly enforcing rules such as minimum cell distance or plausible nuclei volume constraints in a data-driven manner. This is a unique method as it keeps the number of manual hyper-parameters tuning to a minimum and can be improved over time as more validated and corrected datasets are incorporated in the training set.

To assemble the predicted tree, nuclei labels in each frame are connected to their parents in the previous frame by finding the linking label with the maximum overlap (**Fig 2c, Supplementary Figure 4**). The predicted tree is then saved with the structure of a MaMuT .xml track file, which can be imported into Mastodon for further correction (**Fig 2d**). As a direct consequence of the joint segmentation, additional information such as the nuclei volume can be overlaid on the predicted trees to aid in the curation process (**Supplementary Figure 4**, **Supplementary Note 2**). For instance, jumps in nuclear volume highlight positions where tracks should be merged or split. The manual curation time ranges from minutes to a couple hours on the most challenging datasets (e.g. low SNR images, abnormal nuclei shape). In summary, this novel and efficient tree prediction approach allows high quality prediction of organoid lineage trees with long tracks spanning multiple division cycles (up to 5 generations in this work) enabling tracked data to cross spatiotemporal scales.

Digital organoid viewer

With the lineage trees and the deep learning 4D segmentation of organoid, lumen, cells and nuclei at hand, we created a multiscale digital organoid viewer to explore and perform in-depth data mining. The viewer combines both lineage trees and segmented meshes, facilitating the direct comparison of different features within a multiscale digital organoid framework. We also added the possibility to overlay recorded images with the meshes allowing a direct inspection of the predicted segmentation (**Fig 3a, Supplementary Movie 2**). When hovering a node with the mouse, its associated features are displayed, selected nodes are interactively highlighted on the meshes, and color coding of both trees and meshes can be assigned independently, so that same or complementary features can be visualized at once.

As an example of the analysis and visualization tools presented above, nuclear volume quantifications can be evaluated directly onto the tree of a specific dataset (**Fig 3b**). Using this approach, it is possible to observe and quantify how much nuclei volumes change with each generation and over time, with the smallest volumes observed right after division. Similarly, we can observe that the nuclear distance to the basal membrane (**Fig 3c**) increases due to interkinetic nuclear migration towards the apical side. Combining the same visualization procedure with the segmented meshes, we can render the nuclei or cells in 3D, using the same color-coding as for feature on the trees (**Fig 3d**). Last but not least, we can also compare the extracted features against the general trend from all other datasets combined, allowing us a direct evaluation of variability across experiments (**Fig 3e,f**). This way we can for example evaluate the increased distancing of nuclei from the apical membrane, a known effect due to epithelial polarization (**Fig 3f**).

In summary, this is a unique set of tools which allows not only multiscale segmentation of organoids along with lineage tree predictions, but also the simultaneous visualization of both

trees and segmented meshes into a unified web-viewer. All steps of the process are implemented to keep storage, memory, and manual tuning requirements to a minimum, making this a powerful and yet lightweight light-sheet based framework.

Functional imaging through fixation and backtracking

Next, we analyzed functional information on the tracked cells and organoids contained in the lineage trees. Although our imaging framework allows the visualization and quantification of a large number of features at the cellular and organoid levels throughout organoid growth, functional information remains dependent on the currently existing fluorescent organoid lines. The easiest way to theoretically approach this is to perform stable multicolor live imaging for long periods of time. However, overlapping emission/excitation spectra limits the total number of fluorescent reporters and concerns regarding interference with the normal cell function, signal-to-noise sensitivity for low abundant proteins, photostability and general phototoxicity due to laser illumination limit the use of fluorescent reporters. To overcome this, we integrated fixation and immunolabelling steps after the live recordings in order to assess the end state of cells. Moreover, we combined immunolabelling information at the last time-point with the time-lapse recording by tracking the immunolabelled cells back through the lineage tree (**Fig 4a**), using LSTree for further visualization and analysis.

For fixation we fixed the sample at the end of the recording with 4% PFA, before continuing with the immunolabelling protocol (see **Methods Section**). Here the pre-patterning of the FEP foil holding the sample was crucial, as without it the Matrigel drops could be easily washed out. To best account for possible organoid drifts, we imaged the entire fixation procedure, so that we could keep track of the organoids during fixation, leading to a recovery after fixation success rate of more than 80%.

On the tissue level, to register the fixed organoids back to their shape at the last time-point of the live recording we used similarity transformations implemented in ITK and available via Elastix[20,21] (used as a stand-alone tool. For more information, please refer to the **Methods Section**). As a first example we imaged H2B-mCherry, mem9-GFP organoids until day 3 (**Supplementary Movie 3** left). It has been shown that between around day 1.5 intestinal organoids break symmetry through the appearance of the first differentiated cells of the secretory lineage (Paneth cells, Lysozyme). Preceding the appearance of Paneth cells there is the local establishment of a Notch-Delta lateral inhibition event, with future Paneth cells being typically Delta Like Ligand 1 positive (DLL1+)[6] . To analyze symmetry breaking, we fixed the organoids at 56 hours and stained for DLL1-Alexa488 and Lys-Alexa647. A cyst was registered to its shape before fixation (as exemplified in **Fig 4b**) and two DLL1+ cells were found (one of them also Lys+), which were followed back over the entire lineage tree while observing their relative position on the segmentation meshes (**Fig 4c-e**, **Supplementary Movie 3** right). Intriguingly, the two DLL1+ cells are two sister cells that were formed at the end of the division from generation 5 to generation 6, around 10 hours before fixation.

Since both cells show DLL1 but only one is Lys+, one hypothesis was that before generation 5 the cell already starts differentiating towards the secretory lineage (DL11+), but after division one of the daughter cells is differentiating to Paneth cell (Lyz+). To follow cellular dynamics and changes of features of these specific cells in their spatial environment we analyzed nuclei and cell volumes (extracted with LSTree) per generation of the backtracked cells from generation 5 and 6 and compared them to all of the other cells during the same generations

262 (**Fig 4f**). Interestingly, cellular and nuclear volumes of the backtracked cells do not seem to
263 deviate relative to each other during generation 5. After cell division and entering generation
264 6, however, the nuclei volumes of both DLL1+ sister cells show an increased relative
265 difference to one another, with the Lys+ cell having a slightly larger nucleus.

266 Next, we evaluated the dynamics of neighbor exchange by cross-checking the closest cells to
267 a backtracked cell(s) of interest at each time-point with LSTree. We examined if the progeny
268 of these two sister cells had high level of mixing with other cells during cyst growth. From the
269 visualization of the tracked neighbors on the lineage tree and segmented meshes (**Fig 4g**), it
270 is apparent that neighbor exchanges, although distributed across the tree, do not happen
271 often nor with many different cells, keeping an average of 5 cells.

272 The above results show that, by combining our light-sheet framework with standard fixation
273 and registration techniques we can broaden the level of functional information, bridging it to
274 the dynamical processes during live imaging. Consequently, we were capable of dissecting
275 some initial dynamical elements preceding the formation of DLL1+ and Paneth cells in the
276 context of the entire organoid development, analyzing the process of symmetry-breaking
277 events across biological scales.
278

279 ## Nuclei merging events during organoid growth

280 From our backtracking example we noticed that one cell undergoes multiple rounds of failed
281 division, with two daughter cells merging before a new division starts (**Fig 5a**). Upon further
282 inspection of the other 6 lineage trees, we realized that the majority of the datasets contained
283 at least one merging event during early phase of organoid growth whereby two sister nuclei,
284 at the end of their cell cycle, divided again into two instead of into four nuclei. To investigate
285 whether a failed division during the previous mitotic cycle was causing these nuclei merging,
286 we examined the last step of the previous cell division. In all cases there was a problem during
287 late cytokinesis, with the two sister cells never fully separating (**Fig 5a,b**). Nuclear volume for
288 all the daughters arising after the merging event is clearly increased and cell volume followed
289 the same behavior, roughly doubling in tetraploid cells (**Fig 5c,d**). To dismiss the possibility
290 that these mitotic failures are caused by phototoxic effects of the imaging itself, we
291 performed a time-course experiment with wild-type organoids grown from single cells under
292 same medium conditions as the live recordings. We fixed organoids at days 2 and 3, staining
293 them for e-Cadherin and DAPI to have comparable visual information. Despite the lack of
294 continuous illumination, the resulting data showed many cysts with polynucleated cells, as
295 well as cells with enlarged nuclei (**Fig 5e**).

296 Surprisingly, the progeny of a cell that underwent cytokinesis failure can lead to cells that
297 remain part of the epithelium until the end of the recordings, when we can observe fully
298 budded organoids or mature enterocysts (end of day 4) (**Fig 5f,g**). Yet, comparing to
299 unaffected parts of the trees, this binucleation progeny typically has higher probability to be
300 extruded into the lumen (~46% for merged progeny against ~5% for other cells). Another
301 intriguing observation is that the remaining 54% of the cells are not localized to the crypt but
302 to the villus (**Fig 5f**, **Supplementary Fig 5**). This is an interesting result, as it suggest that there
303 are mechanisms to maintain tissue integrity in the stem cell niche avoiding damaged cells in
304 the crypt.

305 Molecularly, it is known that the Large tumor suppressor kinase 1 (Lats1) can influence
306 cytokinesis failure via lack of inhibition of Lim kinase 1 (Limk1)[22-24]. This poses an interesting

hypothesis on the role of mitotic failure in regeneration as LATS1 and Yap1 are master regulators of regenerative response of the intestinal epithelium. Analysis of RNAseq from previous studies[6], show decrease in Lats1 expression during initial days of organoid growth. The first days of organoid growth recapitulate the regenerative response by upregulating Yap1 and downregulating Lats1. Lats1 perturbations and a time-course imaging of Lats1 double knockouts[6] showed several cysts with double nucleated cells that result from mitotic failures (**Fig 5h**). To further perturb the system at another level, we maintained Yap1 activation through inhibition of RXR[7] and we observed consistent problems during mitosis, including cytokinetic failures (**Fig 5i**), where daughter nuclei come together after being fully separated (**Supplementary Movie 4**).

Taken together, through the multi scale approach of 3D segmentation, feature extraction and lineage tree analysis we were able to identify consistent polyploidy events during early intestinal organoid development and the fate of their progeny. Our framework allowed us to bridge the observed mitotic defects across scales towards the tissue scale, showing the end fate of the merged cells progeny and spatially locating them onto the mature organoid morphology. This is shedding new light on the robustness of a regenerative YAP cellular state, questioning the role of polyploidy in intestinal regeneration.

Discussion

Here we have presented a unified light-sheet imaging framework tailored to intestinal organoid development. Named LSTree, it is a comprehensive and light-weight approach that uniquely combines image pre-processing, single cell tracking in the form of entire lineage trees and multiscale segmentation and feature extraction along with a dedicated unified visualization and analysis tool. The framework encompasses pre- and post-processing tools for cropping/registration, denoising and deconvolution with combined on the fly compression, generating high-quality datasets with minimal storage costs. We show that this framework is capable of fully segmenting and tracking intestinal organoids as they grow from single cells for several days, bridging biological scales to the point when the organoid has hundreds of cells. Information on organoid, lumen, cell and nuclei volumes along with other multivariate features can be simultaneously visualized with the lineage tree data and further analyzed through a web-based Digital Organoid Viewer, facilitating a more global understanding of the dynamics acquired at subcellular resolution. The use of specialized neural networks dedicated to multiscale segmentation and lineage tree predictions allow the framework to be plastic enough to handle different kinds of live-imaging data as well as continuously improve through the utilization of dedicated tools for retraining of the models. Furthermore, the training architectures keep the number of parameters and computational resources to a minimum, relieving the needs for any highly specialized IT infra-structure, as they can be directly used on off-the-shelf workstations.

We pushed the usability of our framework a step further by combining it with standard fixation techniques after live imaging via the development of sample holder patterned with a cold stamp technique, allowing the tracking of immunolabelled cells back in time and space and compare their features to all of the other cells over the entire organoid growth. Unlike

350 lineage tracing in single cell RNA sequencing, which clusters cells only by their RNA phenotypic
351 fingerprint or a barcode[25], with our approach we can focus on the missing spatiotemporal
352 organization in a causal way, as we follow the same cells over time. Consequently, we can
353 now address, in unprecedented detail, the evolution of cells that can give rise to the first
354 symmetry breaking event, keeping track of local interaction within the whole organoid.

355 Last but not least, we present for the first time the appearance of cells having cytokinesis-
356 related mitotic errors leading to binucleation during early organoid growth. With LSTree we
357 were able of rapidly verifying these errors across a multitude of different long-term
358 recordings, showing that they are a consistent feature during early cyst growth. Interestingly,
359 polyploidy has been associated with wound healing after injury[26]. In the liver, polyploid cells
360 seem to have a tumor-supressor role with polyploid cells occurring mostly due to cytokinesis
361 failure and endoreduplication[27,28]. However, polyploid hepatic cells are mostly quiescent and
362 do not divide unless the liver undergoes regenerative process due to a lesion. In contrast, our
363 observed bi-nucleated cells do not undergo cell cycle arrest, but continue to divide for even
364 multiple cycles, either with or without repeated clear mitotic failure. We also show that
365 although these cells may appear in the crypt region during crypt formation (during days 3-4),
366 they typically do not manage to reside in the crypt, whereas cells in the villus region remain
367 part of the epithelium. Similar mitotic errors are also shown with inducible Lats-DKO intestinal
368 organoid lines, as well as in the condition of YAP1 overexpression through inhibition of RXR.
369 Since Lats has a direct implication during cytokinesis, we propose that during organoid growth
370 and intestinal regeneration there must be a balance between high-proliferative regenerative
371 state – which is more error prone – and a counteracting checkpoint at the tissue scale to avoid
372 mutations in the stem cell compartment. This way tissue integrity can be achieved fast, with
373 any remaining mutations in the villus being eventually shed off via e.g. anoikis when cells
374 reenter homeostasis.

375 In conclusion, with LSTree we can cross biological scales with unprecedented detail, as we can
376 follow particular subcellular behaviors while keeping track on the entire tissue development
377 over long periods of time. The usability of the tools presented can go far beyond the examples
378 shown here, as they can be compatible with different light-sheet modalities making this
379 framework also very useful in the study of other 3D cell cultures. In fact, we believe that the
380 LSTree is a first step towards a comprehensive and quantitative framework dedicated to the
381 creation of fully digital organoid maps, so that the intrinsic culture variabilities can be
382 overcome with the creation of averaged organoids to be used as landmarks for future studies.

383

384 Methods

385 Organoid lines

386 All animal experiments were approved by the Basel Cantonal Veterinary Authorities and
387 conducted in accordance with the Guide for Care and Use of Laboratory Animals. Male and
388 female outbred mice between 7 and 15 weeks old were used for all experiments. Mouse lines
389 used: C57BL/6 wild type (Charles River Laboratories), H2B-mCherry C57BL/6 x C3H F1 females
390 heterozygous for H2B-mCherry (kind gift from T. Hiragi lab, EMBL), Lats1Δ/Δ; Lats2Δ/Δ (LATS
391 DKO, kind gift from Jeff Wrana, Department of Molecular Genetics, University of Toronto,

392 Canada)[29]. For H2b-mCherry/mem9-GFP organoids, H2b-mCherry organoids were infected
393 with LV.EF1.AcGFP1-Mem-9 lentivirus particle (Clontech, Takara Bio USA).
394

395 **Organoid culture**

396 Organoids were generated from isolated crypts of the murine small intestine as previously
397 described[5]. In brief, the section of the initial part of the small intestine was opened
398 lengthwise, cleaned with cold PBS and, after removal of villi by scraping with a cold glass slide,
399 sliced into small fragments roughly 2 mm in length. The tissue was then incubated in 2.5 mM
400 EDTA/PBS at 4 °C for 30 min with shaking. Supernatant was removed and pieces of intestine
401 were re-suspended in DMEM/F12 with 0.1% BSA. The tissue was then shaken vigorously. To
402 collect the first fraction, the suspension was passed through a 70 µm strainer.

403 The remaining tissue pieces were collected from the strainer and fresh DMEM/F12 with 0.1%
404 BSA was added, followed by vigorous shaking. The crypt fraction was again collected by
405 passing through a 70 µm strainer. In total, 4 fractions were collected. Each fraction was
406 centrifuged at 300g for 5 min at 4 °C. Supernatant was removed and the pellet was re-
407 suspended into Matrigel with medium (1:1 ratio) and plated into 24 well plates. Organoids
408 were kept in IntestiCult Organoid Growth Medium (STEMCELL Technologies) with 100 µg/ml
409 Penicillin-Streptomycin for amplification and maintenance.

410

411 **Time course experiments of fixed organoid samples**

412 Organoids were collected 5-7 days after passaging and digested with TrypLE (Thermo Fisher
413 Scientific) for 20 min at 37 °C. Dissociated cells were passed through a cell strainer with a pore
414 size of 30 µm (Sysmex). For all experiments, single alive cells were sorted by FACS (Becton
415 Dickinson FACSAria cell sort or Becton Dickinson Influx cell sorter). Forward scatter and side
416 scatter properties were used to remove cell doublets and dead cells. Sorted cells were collected
417 in ENR medium composed of advanced DMEM/F-12 with 15mM HEPES (STEM CELL Technologies)
418 supplemented with 100 µg/ml Penicillin-Streptomycin, 1×Glutamax (Thermo Fisher Scientific),
419 1×B27 (Thermo Fisher Scientific), 1xN2 (Thermo Fisher Scientific), 1mM N-acetylcysteine (Sigma),
420 500ng/ml R-Spondin (kind gift from Novartis), 100 ng/ml Noggin (PeproTech) and 100 ng/ml
421 murine EGF (R&D Systems). Collected cells were mixed with Matrigel (Corning) in a medium to
422 Matrigel ratio of 1:1. In each well of a 96 well plate, 3µl droplets with ca. 3000 cells were seeded.
423 After 20 min of solidification at 37 °C, 100 µl of medium was overlaid. From day 0 to day 1, ENR
424 was supplemented with 20% Wnt3a-conditioned medium (Wnt3a-CM), 10 µM Y-27632 (ROCK
425 inhibitor, STEMCELL Technologies) and 3 µM of CHIR99021 (GSK3B inhibitor, STEMCELL
426 Technologies, cat # 72054). From day 1 to 3 ENR was supplemented with 20% Wnt3a-CM and 10
427 µM Y-27632. From day 3 to 5, only ENR was added to the cells. Wnt3a-CM was produced in-house
428 by Wnt3a L-cells (kind gift from Novartis).

429

430 **Fixed sample preparation and time-course imaging**

431 Organoids are embedded in a Matrigel droplet. Due to the nature of the droplet, individual
432 organoids are located at different heights in the Matrigel drop. To allow imaging of all
433 organoids within a similar z-range, each 96-well plate was centrifuged at 3000 rpm for 10 min
434 in a pre-cooled centrifuge at 10 °C prior to fixation. Organoids were fixed in 4% PFA (Electron
435 Microscopy Sciences) in PBS for 45 min at room temperature. For time course and compound

experiments, organoids were permeabilized with 0.5% Triton X-100 (Sigma-Aldrich) for 1 h and blocked with 3% Donkey Serum (Sigma-Aldrich) in PBS with 0.1% Triton X-100 for 1 h. For the images in Figure 5e, membrane staining with E-Cadherin (BD Biosciences, # 610182) was done at 1:300 ratio in Blocking buffer for 20 hours at 4°C. DAPI staining was performed at concentration of 300nM for 30 min at room temperature. All secondary antibodies were added at 1:300 for 1 hour in room temperature. Cell nuclei were stained with 20 µg/ml DAPI (4',6-Diamidino-2- Phenylindole, Invitrogen) in PBS for 15 min. High-throughput imaging was done with an automated spinning disk microscope from Yokogawa (CellVoyager 7000S), with an enhanced CSU-W1 spinning disk (Microlens-enhanced dual Nipkow disk confocal scanner), a 40x (NA = 0.95) Olympus objective, and a Neo sCMOS camera (Andor, 2,560 × 2,160 pixels). For imaging, an intelligent imaging approach was used in the Yokogawa CV7000 (Search First module of Wako software). For each well, one field was acquired with 2x resolution in order to cover the complete well. This overview fields were then used to segment individual organoids on the fly with a custom written ImageJ macro which outputs coordinates of individual organoid positions. These coordinated were then subsequently imaged with high resolution (40x, NA = 0.95). For each site, z-planes spanning a range up to 140 µm were acquired. For the data in Figure 5e 2 µm z-steps were used.

Inhibition experiments

Lats-DKO

Analysed data stems from a previous publication[6], with Lats DKO organoids dissociated into single cells and plated into 96 well plates, fixed and stained with DAPI following the published protocols. Tamoxifen induction (1:1000) was kept in the medium until fixation time.

RXRi

RXR inhibition was achieved by adding the Cpd2170 RXR antagonist[7] compound at 1:2000 ratio to the medium from the moment single cells were seeded onto the light-sheet holder. The compound was kept throughout the data acquisition. Organoids used for this experiment had been infected with H2B-iRFP670 for live nuclei labeling.

Light-sheet recordings

Sample preparation

H2b-mCherry / mem9-GFP and H2B-iRFP670 organoids were collected and digested with TrypLE (Thermo Fisher Scientific) for 20 min at 37 °C. Alive double positive (mCherry/GFP) cells were sorted by FACS and collected in medium containing advanced DMEM/F-12 with 15 mM HEPES (STEM CELL Technologies) supplemented with 100 µg/ml Penicillin-Streptomycin, 1×Glutamax (Thermo Fisher Scientific), 1×B27 (Thermo Fisher Scientific), 1xN2 (Thermo Fisher Scientific), 1mM N-acetylcysteine (Sigma), 500ng/ml R-Spondin (kind gift from Novartis), 100 ng/ml Noggin (PeproTech) and 100 ng/ml murine EGF (R&D Systems). 2500 cells were then embedded in 5ul drop of Matrigel/medium in 60/40 ratio. Drops were placed in the imaging chamber and incubated for 20 min before being covered with 1ml of medium. For the first three days, medium was supplemented with 20% Wnt3a-CM and 10 µM Y-27632 (ROCK inhibitor, STEMCELL Technologies). For the first day, in addition, 3µM of CHIR99021

478 (STEMCELL Technologies) were supplemented. After 2 hours incubation in a cell culture
479 incubator the imaging chamber was transferred to the microscope kept at 37C and 5% CO2.

480 **Imaging**

481 For all light-sheet experiments a LS1-Live dual illumination and inverted detection microscope
482 from Viventis Microscopy Sàrl was used. Different single cells were selected as starting
483 positions and imaged every 10 min for up to 5 days. A volume of 150 -200µm was acquired
484 with a Z spacing of 2µm between slices and 100 ms exposure time for each slice. Laser
485 intensity was kept to a minimum necessary to still obtain reasonable signal to noise from the
486 raw data, while keeping phototoxicity to a minimum possible. Medium was exchanged
487 manually under the microscopy every day.

488

489

490 ## Fixation on time-lapse recordings

491 Organoids are embedded in 5 µm Matrigel droplets which are deposited at equal distances
492 on top of the FEP foil of the light-sheet sample holder. After live imaging is done, the medium
493 is replaced by 4% PFA in PBS, and left in the chamber for maximum 30 minutes at 37°C in the
494 microscope. After fixation the organoids were permeabilized with 0.5% Triton X-100 (Sigma-
495 Aldrich) for 1 h and blocked with 3% Donkey Serum (Sigma-Aldrich) in PBS with 0.1% Triton
496 X-100 for 1 h. For the images in Figure 4, the cyst was stained with DLL1 antibody (R&D
497 Systems, # AF3970) at 1:100 ratio and left overnight at 4°C. For Lysozyme (Dako, # A0099) we
498 used a 1:400 ratio for 3 hours at room temperature.

499

500 ## Registration for back-tracking after fixation of time-lapses

501 Since PFA fixation causes the Matrigel droplet to flatten, we perform imaging while fixation
502 is taking place. Typically we observe no change within the first 5 minutes, whereas after that
503 there is a sudden increase in organoid movement towards the bottom of the sample holder.
504 To take this into account, we increased the imaging volume and step size to be able to
505 encompass a larger volume and still track the organoid. For the data in Figure 4 we increased
506 stack size from 150 µm and 2 µm step size to 300 µm at 3 µm step size. However, larger values
507 can also be used.

508 Nonetheless, the flattening of the droplet will lead the organoids to rotate or translate in
509 space. Furthermore, PFA fixation also changes the shape of tissue samples by shrinking or
510 swelling. To bridge the translational, rotational and rescaling of the organoids during fixation
511 procedures, we registered fixed organoids using Elastix v4.900 (https://elastix.lumc.nl/). Since
512 Elastix can be directly installed from the repository as pre-compiled libraries, we refrained
513 from embedding the registration into LSTree, and left it as a stand-alone tool. For all
514 registrations using the similarity transform, a base parameter file set for performing similarity
515 transformations was used and eventually modified so that best results could be achieved.

516

517 ## LSTree modules

518 Pre-processing steps rely mostly on cropping and registration, denoising, and deconvolution
519 steps. Although not part of LSTree itself, improvements in the microscope software (on-the-

fly LZW compression, position dependent illumination alignment) were performed in collaboration with Viventis Microscopy Sàrl and are now part of their current microscope software.

Detailed information regarding pre-processing, segmentation strategies and feature extraction can be found in **Supplementary Text.**

Acknowledgements

We thank M. Rempfler for helpful discussions on framework implementation and support, D. Vischi, E. Tagliavini and Sjoerd van Eeden for IT support, Q. Yang for discussions on pre-processing, S. Xie for helpful discussions on biological aspects, A. Peters for light-sheet, I. Lukonin for help with RXR compound, H. Kohler for sorting, P. Argast for help with building the FEP foil aluminum stamp, C. Tsiairis, L. Gelman and laboratory members for reading the manuscript. Funding: EMBO (ALTF 571-2018 to G.M.), SNSF (POOP3_157531 to P.L.). This work received funding from the ERC under the European Union's Horizon 2020 research and innovation programme (grant agreement no. 758617).

Author information

Author notes

These authors contributed equally: Gustavo de Medeiros, Raphael Ortiz

Affiliations

Friedrich Miescher Institute for Biomedical Research (FMI), Basel, Switzerland

Gustavo de Medeiros, Raphael Ortiz, Francisca Maurer & Prisca Liberali

University of Basel, Basel, Switzerland

Prisca Liberali

Viventis Microscopy Sàrl, EPFL Innovation Park, Lausanne, Switzerland

Andrea Boni, Petr Strnad

Contributions

P.L. and G.M. conceived and P.L. supervised the study, P.L., G.M., and A.B. designed the experiments, F.M., G.M. cultured the organoids, G.M. and A.B. recorded the time-lapses, P.S. wrote and implemented compression and position dependent illumination code into microscope software, A.B. created first Mastodon trees, R.O. wrote LSTree framework with the support of G.M., G.M. performed time-course experiment. G.M., R.O. and P.L. analysed the data, G.M., R.O. and P.L. wrote the paper.

Corresponding author

Correspondence to Prisca Liberali.

Ethics declarations

Competing interests

A.B. and P.S. are co-founders of Viventis Microscopy Sàrl that commercializes the light-sheet microscope used in this study.

References

1 Mayr, U., Serra, D. & Liberali, P. Exploring single cells in space and time during tissue development, homeostasis and regeneration. *Development* **146**, dev176727, doi:10.1242/dev.176727 (2019).

2 Zinner, M., Lukonin, I. & Liberali, P. Design principles of tissue organisation: How single cells coordinate across scales. *Current Opinion in Cell Biology* **67**, 37-45, doi:10.1016/j.ceb.2020.07.004 (2020).

3 Xavier Da Silveira Dos Santos, A. & Liberali, P. From single cells to tissue self-organization. *The FEBS Journal* **286**, 1495-1513, doi:10.1111/febs.14694 (2019).

4 Bankaitis, E. D., Ha, A., Kuo, C. J. & Magness, S. T. Reserve Stem Cells in Intestinal Homeostasis and Injury. *Gastroenterology* **155**, 1348-1361, doi:10.1053/j.gastro.2018.08.016 (2018).

5 Sato, T. *et al.* Single Lgr5 stem cells build crypt–villus structures in vitro without a mesenchymal niche. *Nature* **459**, 262-265, doi:10.1038/nature07935 (2009).

6 Serra, D. *et al.* Self-organization and symmetry breaking in intestinal organoid development. *Nature* **569**, 66-72, doi:10.1038/s41586-019-1146-y (2019).

7 Lukonin, I. *et al.* Phenotypic landscape of intestinal organoid regeneration. *Nature* **586**, 275-280, doi:10.1038/s41586-020-2776-9 (2020).

8 Yang, Q. *et al.* Cell fate coordinates mechano-osmotic forces in intestinal crypt morphogenesis. *bioRxiv pre-print server*, doi:10.1101/2020.05.13.094359 (2020).

9 Alladin, A. *et al.* Tracking cells in epithelial acini by light sheet microscopy reveals proximity effects in breast cancer initiation. *eLife* **9**, doi:10.7554/elife.54066 (2020).

10 Kok, R. N. U. *et al.* OrganoidTracker: Efficient cell tracking using machine learning and manual error correction. *PLOS ONE* **15**, e0240802, doi:10.1371/journal.pone.0240802 (2020).

11 Hof, L. *et al.* Long-term live imaging and multiscale analysis identify heterogeneity and core principles of epithelial organoid morphogenesis. *BMC Biology* **19**, doi:10.1186/s12915-021-00958-w (2021).

12 Dumortier, J. G. *et al.* Hydraulic fracturing and active coarsening position the lumen of the mouse blastocyst. *Science* **365**, 465-468, doi:10.1126/science.aaw7709 (2019).

13 Rossi, G. *et al.* Capturing Cardiogenesis in Gastruloids. *Cell Stem Cell* **28**, 230-240.e236, doi:10.1016/j.stem.2020.10.013 (2021).

14 Krull, A., Buchholz, T.-O. & Jug, F. Noise2Void - Learning Denoising from Single Noisy Images. *arXiv pre-print server*, doi:arxiv:1811.10980 (2019).

15 Czech, E., Aksoy, B. A., Aksoy, P. & Hammerbacher, J. Cytokit: a single-cell analysis toolkit for high dimensional fluorescent microscopy imaging. *BMC Bioinformatics* **20**, doi:10.1186/s12859-019-3055-3 (2019).

16 Ortiz, R., De Medeiros, G., Peters, A. H. F. M., Liberali, P. & Rempfler, M. 434-443 (Springer International Publishing, 2020).

17 Ulman, V. *et al.* An objective comparison of cell-tracking algorithms. *Nature Methods* **14**, 1141-1152, doi:10.1038/nmeth.4473 (2017).

18 Moen, E. *et al. Accurate cell tracking and lineage construction in live-cell imaging experiments with deep learning* (Cold Spring Harbor Laboratory, 2019).

19 Sugawara, K., Cevrim, C. & Averof, M. *Tracking cell lineages in 3D by incremental deep learning* (Cold Spring Harbor Laboratory, 2021).

20 Klein, S., Staring, M., Murphy, K., Viergever, M. A. & Pluim, J. P. W. elastix: A Toolbox for Intensity-Based Medical Image Registration. *IEEE Transactions on Medical Imaging* **29**, 196-205, doi:10.1109/TMI.2009.2035616 (2010).

21 Shamonin, D. Fast parallel image registration on CPU and GPU for diagnostic classification of Alzheimer's disease. *Frontiers in Neuroinformatics* **7**, doi:10.3389/fninf.2013.00050 (2013).

22 Yabuta, N. *et al.* N-terminal truncation of Lats1 causes abnormal cell growth control and chromosomal instability. *Journal of Cell Science* **126**, 508-520, doi:10.1242/jcs.113431 (2013).

23 Yang, X. *et al.* LATS1 tumour suppressor affects cytokinesis by inhibiting LIMK1. *Nature Cell Biology* **6**, 609-617, doi:10.1038/ncb1140 (2004).

24 Lens, S. M. A. & Medema, R. H. Cytokinesis defects and cancer. *Nature Reviews Cancer* **19**, 32-45, doi:10.1038/s41568-018-0084-6 (2019).

25 Wheat, J. C. *et al.* Single-molecule imaging of transcription dynamics in somatic stem cells. *Nature* **583**, 431-436, doi:10.1038/s41586-020-2432-4 (2020).

26 Losick, Vicki P., Fox, Donald T. & Spradling, Allan C. Polyploidization and Cell Fusion Contribute to Wound Healing in the Adult Drosophila Epithelium. *Current Biology* **23**, 2224-2232, doi:10.1016/j.cub.2013.09.029 (2013).

27 Zhang, S. *et al.* The Polyploid State Plays a Tumor-Suppressive Role in the Liver. *Developmental Cell* **44**, 447-459.e445, doi:10.1016/j.devcel.2018.01.010 (2018).

28 Margall-Ducos, G., Celton-Morizur, S., Couton, D., Bregerie, O. & Desdouets, C. Liver tetraploidization is controlled by a new process of incomplete cytokinesis. **120**, 3633-3639, doi:10.1242/jcs.016907 (2007).

29 Gregorieff, A., Liu, Y., Inanlou, M. R., Khomchuk, Y. & Wrana, J. L. Yap-dependent reprogramming of Lgr5+ stem cells drives intestinal regeneration and cancer. *Nature* **526**, 715-718, doi:10.1038/nature15382 (2015).

Main Figures

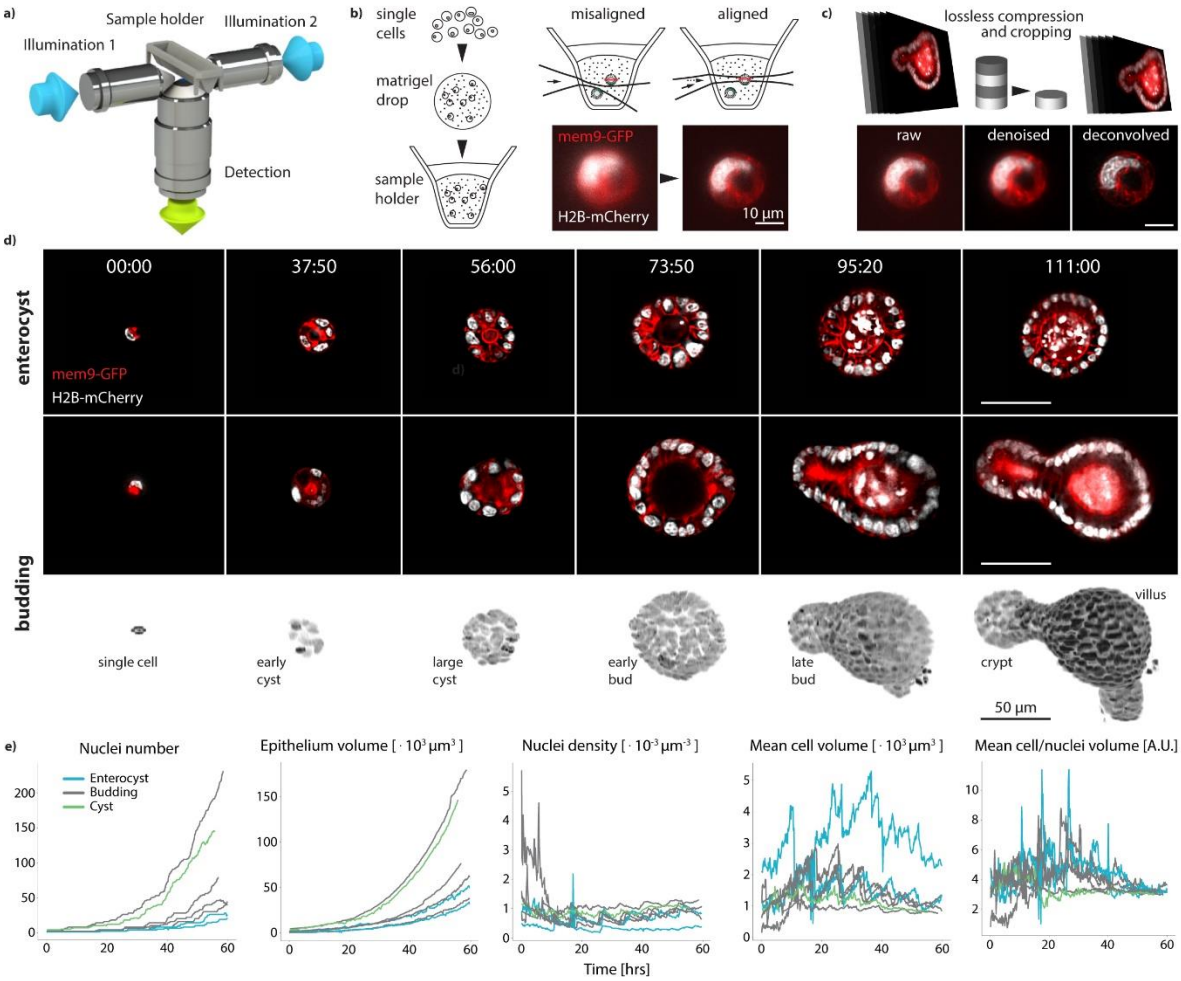

Figure 1: Acquisition of high-resolution 3D organoid images. a) Dual illumination inverted detection light-sheet objective configuration used in all of the recordings. **b)** Left: sample preparation is performed by mixing single cells dissociated from mature organoids with matrigel and depositing 5 uL drops on the light-sheet sample holder. Right: sample position dependent illumination alignment corrects for possible misalignments of the illumination beam in reaching organoids distributed inside the Matrigel drop, improving SNR. **c)** Upper row: minimization of storage needs done with on-the-fly compression and further cropping steps. Lower row: denoising and deconvolution steps further improve image quality. **d)** Time-lapse imaging of organoid growth. Top row shows still images of a growing enterocyst, whereas both lower rows show a stereotypical growth of a budding organoid. **e)** Temporal evolution of nuclei number, epithelium volume, mean cell volume and the ratio between mean cell and mean nuclei volumes for all 7 datasets considered in this work.

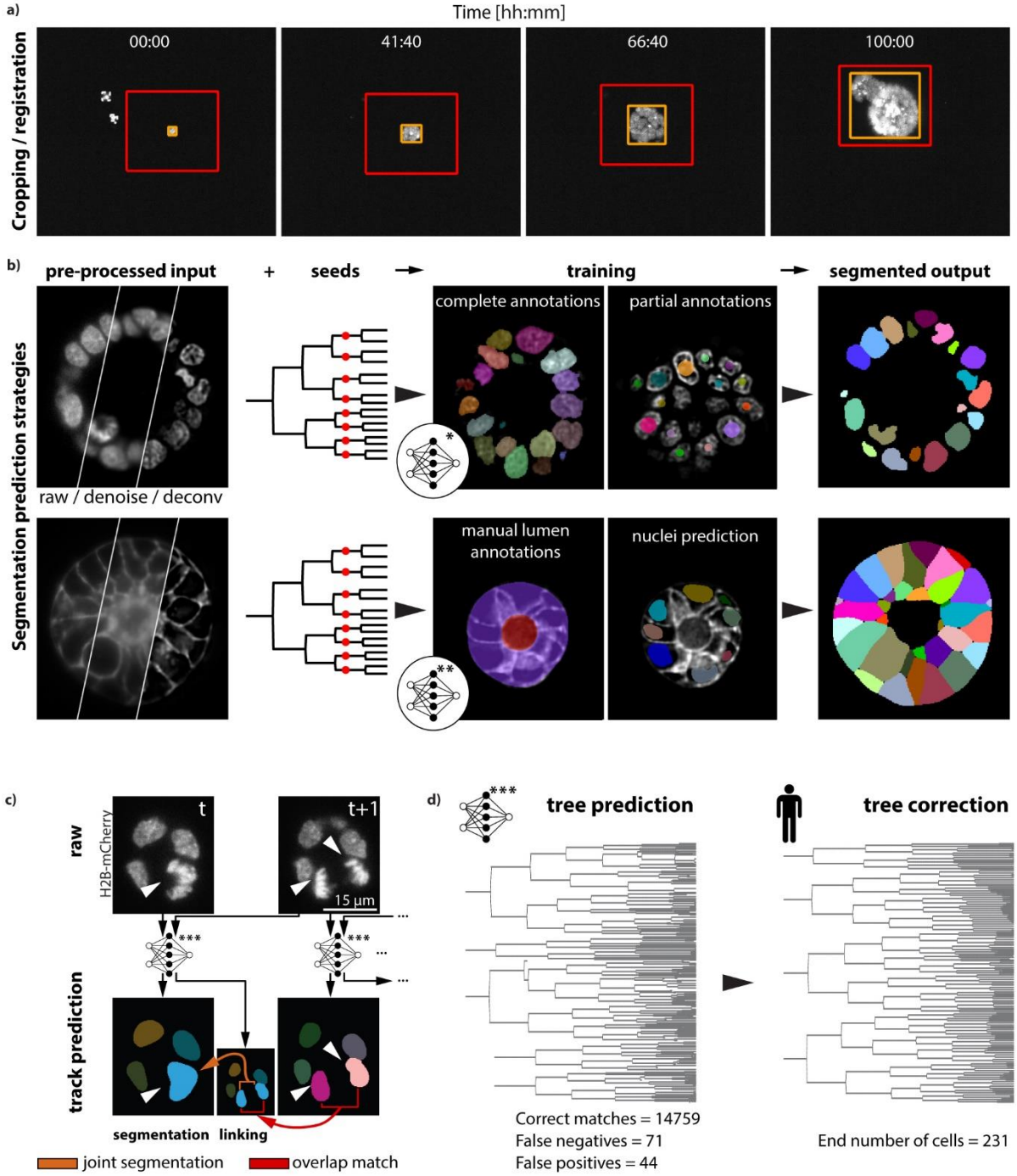

Figure 2: Cropping, segmentation and tree-prediction strategies underlying LSTree. **a)** Cropping of datasets is done in a semi-automatic way: selected object of interest is fitted with an orange (best fit for each particular timepoint) and a global red bounding boxes, which can be corrected in 3D. **b)** Nuclei and cell segmentation strategies. Upper row: denoised and deconvolved input data together with seeds from respective tracking are used as input into the network to predict nuclei volume. The network is trained with both complete and partial annotations. Lower row: Cell volume prediction follows similar input as for nuclei. Main difference is that this second network is trained with supervision of complete manual annotations of lumen and organoid along with the previously done nuclei predictions

themselves. **c)** Strategy for prediction of lineage trees. Track predictions are done with each consecutive pair of frames. Each pair of frames enter the neural network and produce both the timepoint in question and a linking frame which is used to connect to the next timepoint via overlap match. Linking itself is done via joint segmentation. **d)** Example of predicted and corrected tree from a budding organoid dataset with the recording starting from two cells.

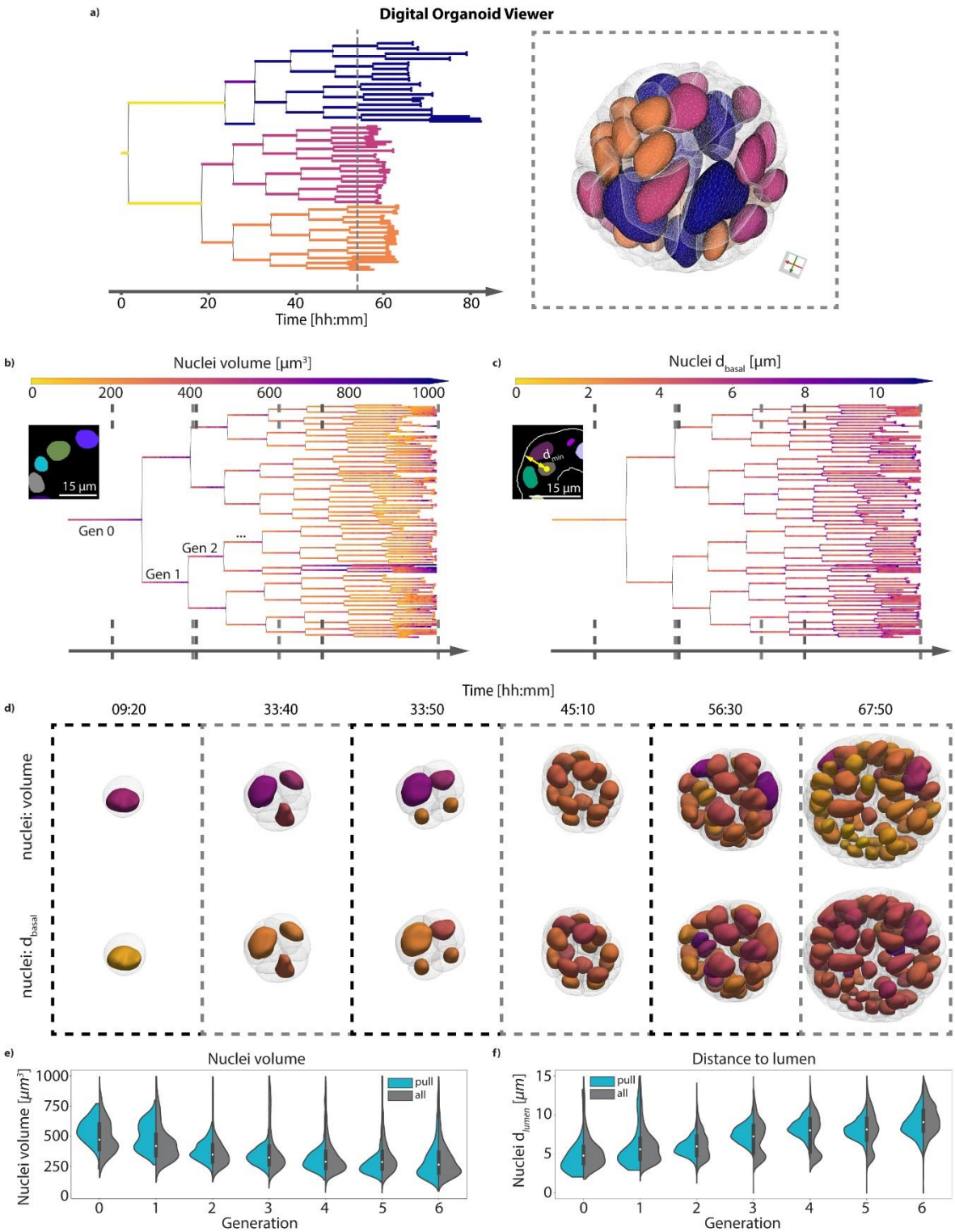

Figure 3: Digital Organoid Viewer. a) Digital organoid viewer is a web-based tool that shows both lineage trees (left) and respective segmented nuclei and cell meshes (right) simultaneously. Color coding of of each data representation can be done in a combined or complementary manner. Here depicted is a color coding based on generation 2, with each of the four cells acquiring different colors being propagated further in time.**b)** Overlay of the nuclei segmentation as predicted in onto the lineage tree. **c)** Overlay of distance to basal

membrane onto the lineage tree. **d)** Visualization of the calculated meshes from nuclei and cell segmentations, overlaying the corresponding values (with corresponding color map) of the features presented in b) and c). The time points chosen are shown via dashed lines on each tree in b) and c). **e,f)** Extracted values for nuclei volume **(e)** and for distance to apical membrane **(f)** of the here exemplified dataset (pull) against all datasets (all) analyzed in this work.

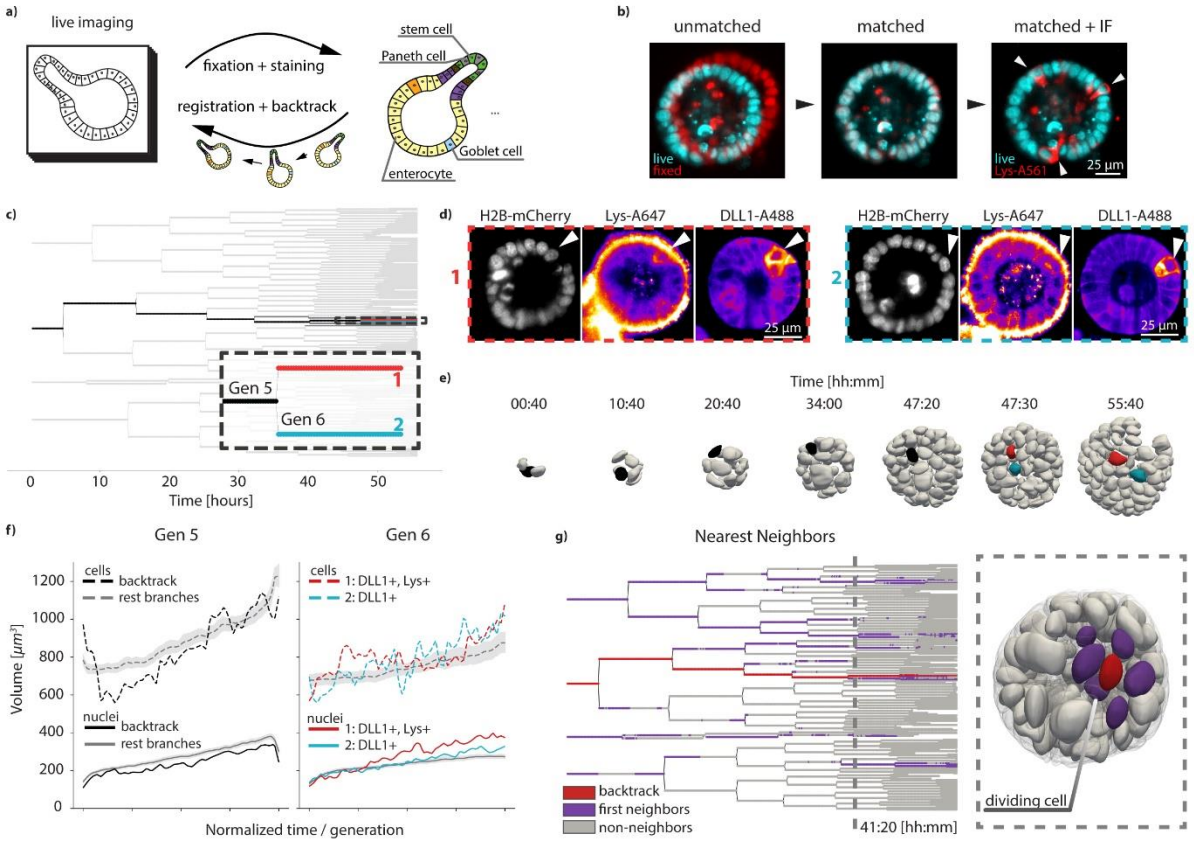

Figure 4: Fixation and backtracking after live-imaging. a) Fixation and backtracking strategy for light-sheet imaging of organoid growth. **b)** After fixation a registration step is needed in order to overlap the fixed nuclei with the nuclei as shown in the last timepoint of the timelapse. Left: midplane of raw data from last time-point H2B-mCherry recording (cyan) against same plane after fixation (red). Center: registration maps the fixed volume into the last time-point volume. Although overlap is not perfect, it is sufficient to maps each nuclei back. Right: After registration additional information from immunolabelling can be overlayed onto last time-point of the live recording, and so cells of interest can be backtracked. **c)** Lineage tree depicting the backtracking of two sister cells. **d)** After fixation, staining for DLL1 and Lysozyme shows two cells expressing these markers. Backtracking of them is shown in a). **e)** Nuclei volume distribution for the backtracked cells against all other cells per generation. **f)** Evaluation of nuclei and cell volumes for the backtracked cells against all other cells during generations 5 and 6, as depicted in c). For all other cells, the mid line corresponds to the mean, whereas the gray region is the standard distribution. **g)** Nearest neighbor evaluation of the backtracked Lys+ cell (red). All nearest neighbors are depicting in magenta, with all remaining cells in gray. Dashed line on the lineage tree is presented as corresponding segmented meshes on the right. A dividing cell can be recognized by the interkinetic movement of its nucleous further apically.

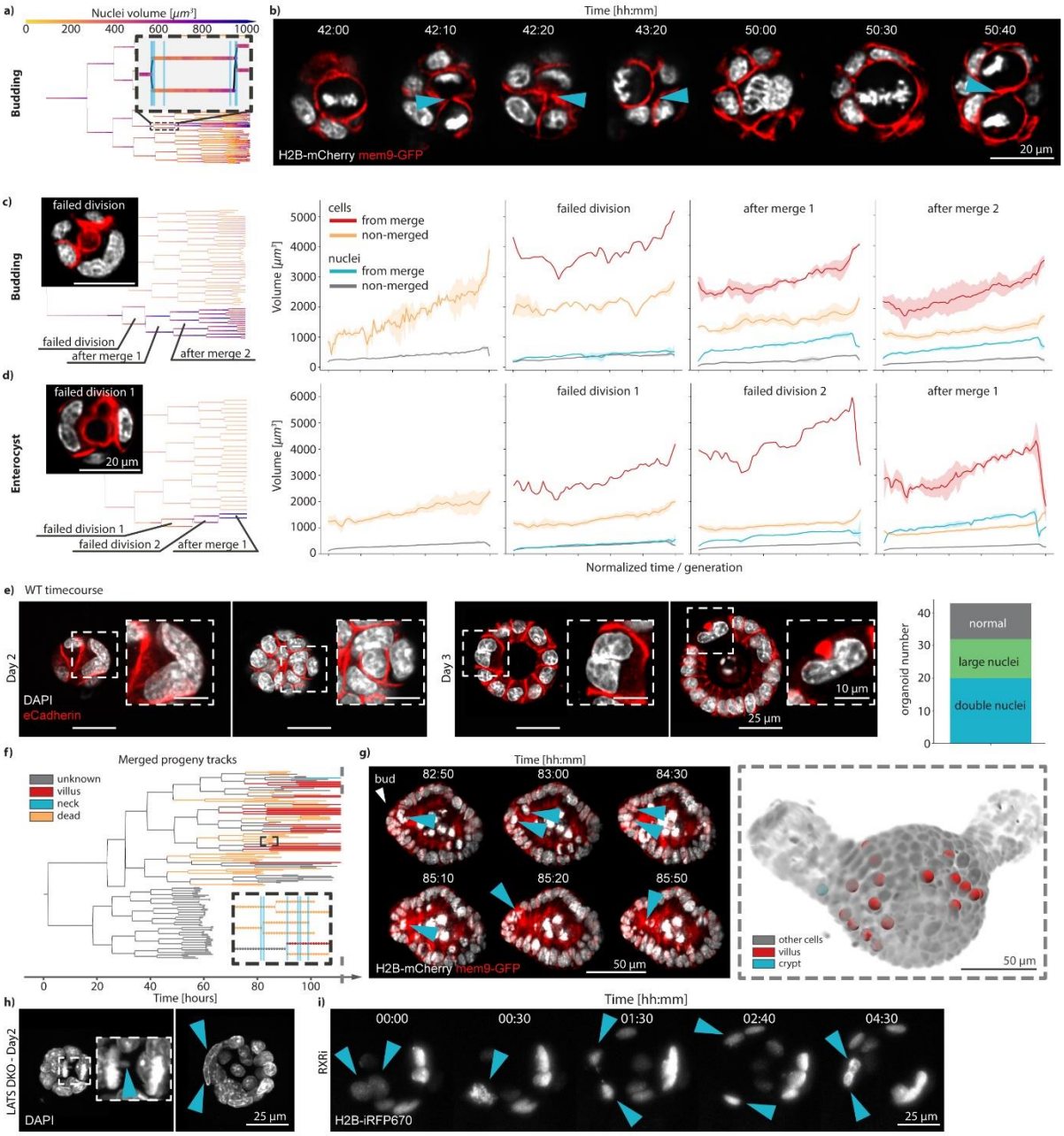

Figure 5: Merging events during early organoid growth. a) Example lineage tree with highlighted insert depicting a cell division where two nuclei divide again into two nuclei. **b)** Still images of the light-sheet recording related to the dataset in a). Cyan arrows mark the position of a connecting region between the two nuclei until the following division occurs, where cytokinesis is successful. Corresponding locations for each depicted timepoint on the lineage tree are shown as cyan lines in the insert in a). **c,d)** Examples of different sequence of events following a failed division during budding organoid and enterocyst growth (left),with quantified nuclei and cell volumes for the highlighted events on the trees (right). **e)** Timecourse data on wild-type intestinal organoids grown from single cells and fixed at days 2 and 3 after seeding. Staining with DAPI and e-Cadherin show binucleated cells and cells with large nuclei, which are quantified on the right. **f)** Left: outcomes from merged progeny and cells from other parts of the tree. No cells part of the merged progeny make it to the crypt. Center: typical outcome of progeny from a failed division; *dead* tracks end with nuclei inside

721 the lumen or basally extruded, *unknown* corresponds to tracks where the high level of cell
722 packing and/or the low quality of the images made it impossible to continue and know their
723 fate, and *alive* corresponds to tracks where the cells are still part of the epithelium until the
724 end of the recording. Right: overlay of tracked cells from left panel onto the last time-point
725 of the recording, showing the spatial organization of the cells in the crypt and vilus regions. **f)**
726 **g)** Major axis length of all nuclei after a failed division (green) and all other cells (gray). **h)**
727 Time-course images of Lats1-DKO organoids at day2. Cyan arrows show lagging chromosome
728 during division (left) and binucleated cell (right). **i)** Still images of an organoid expressing H2B-
729 iRFP670 under RXR inhibitor condition. Cyan arrows follow the moment of cell division of a
730 binucleated cell, with daughter nuclei jumping back to proximity in the end.
731